scientific reports

OPEN

Computational insights into popsilicene as a new planar silicon allotrope composed of 5–8–5 rings

K. A. L. Lima[1], D. A. da Silva[2], F. L. L. Mendonça[3], R. Gargano[4] & L. A. Ribeiro Junior[1,4]✉

Silicon-based two-dimensional (2D) materials have garnered significant attention due to their unique properties and potential applications in electronics, optoelectronics, and other advanced technologies. Here, we present a comprehensive investigation of a novel silicon allotrope, Popsilicene (Pop-Si), derived from the structure of Popgraphene. Using density functional theory and ab initio molecular dynamics simulations, we explore the thermal stability, mechanical and electronic properties, and optical characteristics of Pop-Si. Our results demonstrate that Pop-Si exhibits good thermal stability at 1000 K. Electronic structure calculations reveal that Pop-Si is metallic, with a high density of states at the Fermi level. Furthermore, our analysis of the optical properties indicates that Pop-Si has pronounced UV–Vis optical activity, making it a promising candidate for optoelectronic devices. Mechanical property assessments show that Pop-Si has Young's modulus ranging from 10 to 92 GPa and a Poisson's ratio of 0.95. These results combined suggest its potential for practical applications.

Keywords Popgraphene, Popsilicene, DFT, 2D Materials

Silicon-based technologies have been the cornerstone of modern electronics, powering various devices[1,2], from microprocessors[3,4] to solar cells[5,6]. The discovery and exploration of two-dimensional (2D) materials have opened new avenues for enhancing the performance and capabilities of electronic and optoelectronic devices[7–9]. Among them, silicene[10,11], a single layer of silicon atoms arranged in a honeycomb lattice similar to graphene[12], has garnered considerable interest due to its unique electronic properties, which include a tunable bandgap and high carrier mobility[13]. These properties make silicene a promising candidate for transistors, sensors, and other nanoscale device applications[14].

Recent advances in material synthesis techniques have enabled the production of silicene-based materials[15–18], expanding the possibilities for their use in various technological applications[16,19,20]. Density functional theory (DFT) calculations have been instrumental in predicting the existence and stability of several silicene-based structures, providing insights into their electronic, mechanical, and optical properties[21–28]. These theoretical studies have paved the way for experimental efforts to realize and harness the potential of silicene and its derivatives.

Popgraphene[29], a 2D carbon allotrope characterized by its unique pop-up structure comprising 5–8–5 carbon rings, has shown significant potential for energy storage applications[30,31] due to its unique lattice topology, mechanical strength, and electronic properties[32–36]. Motivated by its success, we propose a silicon version, dubbed Popsilicene (Pop-Si), which retains the structural characteristics of Popgraphene while offering the benefits inherent to silicon-based materials. This study aims to explore the properties of Pop-Si, hypothesizing that it will exhibit a combination of thermal stability, metallic behavior, and unique optical properties with good potential for practical energy storage and conversion applications.

Herein, we present a detailed investigation of Pop-Si using DFT and ab initio molecular dynamics (AIMD) simulations. We explore its electronic and structural properties, including thermal stability at high temperatures, phonon dispersion curves, mechanical properties (elastic constants, Young's modulus, and Poisson's ratio), band structure, and optical characteristics. Our findings demonstrate that Pop-Si is a thermally and dynamically stable

[1]Computational Materials Laboratory, LCCMat, Institute of Physics, University of Brasília, Brasília 70910-900, Brazil. [2]Electrical Engineering - PPEE, University of Brasília, Brasília, Brazil. [3]Department of Electrical Engineering, Faculty of Technology, University of Brasília, Brasília, Brazil. [4]Institute of Physics, University of Brasília, Brasília 70910-900, Brazil. ✉email: ribeirojr@unb.br

metallic material with pronounced UV-Vis optical activity and favorable mechanical properties, making it a strong candidate for various practical applications.

Results

The optimized lattice structure of Pop-Si is depicted in Fig. 1. The bond distances between the highlighted atoms S1–S2, S2–S3, S3–S4, S4–S5, and S5–S6 are measured as 2.29 Å, 2.28 Å, 2.29 Å, 2.28 Å, and 2.24 Å, respectively. These bond lengths are close to those observed in conventional hexagonal silicene, typically around 2.28 Å[37]. Like other 2D silicon materials[38–40], Pop-Si exhibits buckling, with a vertical displacement (ΔZ) of approximately 0.68 Å, similar to the 0.44 Å found in silicene[37]. This buckling is a characteristic feature of silicene and other silicon-based 2D materials, attributed to the sp^3 hybridization of silicon atoms, which contrasts with the planar sp^2 hybridization seen in graphene. The buckling in Pop-Si further aligns it with known properties of silicene, providing additional validation of its structural stability. These similarities suggest that Pop-Si retains the structural characteristics of silicene while adopting a novel configuration.

In the optimized Pop-Si lattice, the lattice vectors are $a = 5.60$ Å and $b = 14.3$ Å, being an orthorhombic crystal structure with the P-1 (CI-1) space group. This structure is different from the hexagonal symmetry of silicene, topologically comprising 5–8–5 fused rings of silicon atoms. Yet, it maintains comparable bond lengths, underscoring the robustness and versatility of silicon-silicon bonds in diverse structural contexts. The formation energy of Pop-Si is calculated to be − 4.57 eV per atom, suggesting that the material is energetically favorable and may be synthesizable under appropriate experimental conditions. This formation energy is comparable to other 2D silicon allotropes reported in the literature.[38–40]. Importantly, the formation energy (E_F) of Pop-Si is calculated as $E_F = E_{total} - nE_{Si}$, where E_F is the total energy of the Pop-Si structure, n is the number of silicon atoms in the material, and E_{Si} is the energy of a Si atom. As mentioned above, the E_F calculation suggests the material's integrity and potential stability. However, calculating the exfoliation energy from first principles[41,42] could offer additional insights, particularly for experimentalists interested in synthesizing Pop-Si.

The thermal and dynamical stability of Popsilicene (Pop-Si) were thoroughly evaluated using AIMD simulations and phonon dispersion analysis. These results, presented in Fig. 2, provide insights into the robustness of Pop-Si under high-temperature conditions and its inherent vibrational properties. To assess the thermal stability, AIMD simulations were performed on a $3 \times 3 \times 1$ supercell (containing 72 atoms) of Pop-Si at 1000 K using an NVT ensemble and the Nosé-Hoover thermostat[43]. The simulations spanned 5 ps with a time step of 1.0 fs.

Figure 2a shows the temporal evolution of the total energy, displaying a nearly flat pattern with minimal fluctuations. This consistency in the total energy suggests the robust thermal stability of Pop-Si. The inset panels in Fig. 2a present top and side views of the final AIMD snapshot. While some deformation in the Pop-Si structure is evident at 1000 K, there is no indication of bond breakage, and the overall configuration remains intact. The deviations observed primarily involve alterations in planarity and bond distances among the lattice atoms attributable to the elevated temperature. This resilience at high temperatures suggests that Pop-Si can maintain its structural integrity under thermal stress, similar to silicene, which exhibits stability at elevated temperatures[44]. The Supplementary Material presents the video from where these AIMD snapshots were extracted.

As mentioned above, phonon dispersion calculations were used to investigate Pop-Si's dynamical stability. These calculations were performed on a $3 \times 3 \times 1$ supercell (containing 72 atoms). Figure 2b presents the phonon dispersion curves for Pop-Si, revealing the absence of imaginary frequencies across the entire Brillouin

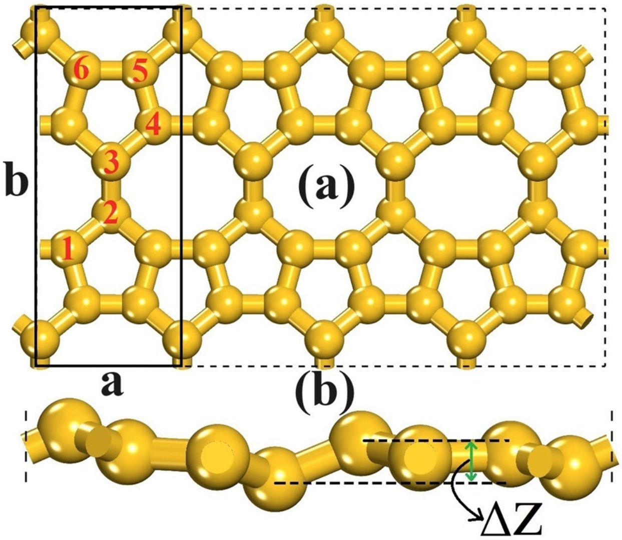

Figure 1. Schematic representation of the Pop-Si sheet. Panels (**a**) and (**b**) present its top and side views, respectively. The black rectangle in panel (**a**), defined by lattice vectors $a = 5.60$ Å and $b = 14.3$ Å, highlights the unit cell. In panel (**b**), one can note that Pop-Si has a buckled structure with width $\Delta Z = 0.68$ Å. The red numbers highlight silicon atoms that form distinct bonds in the lattice.

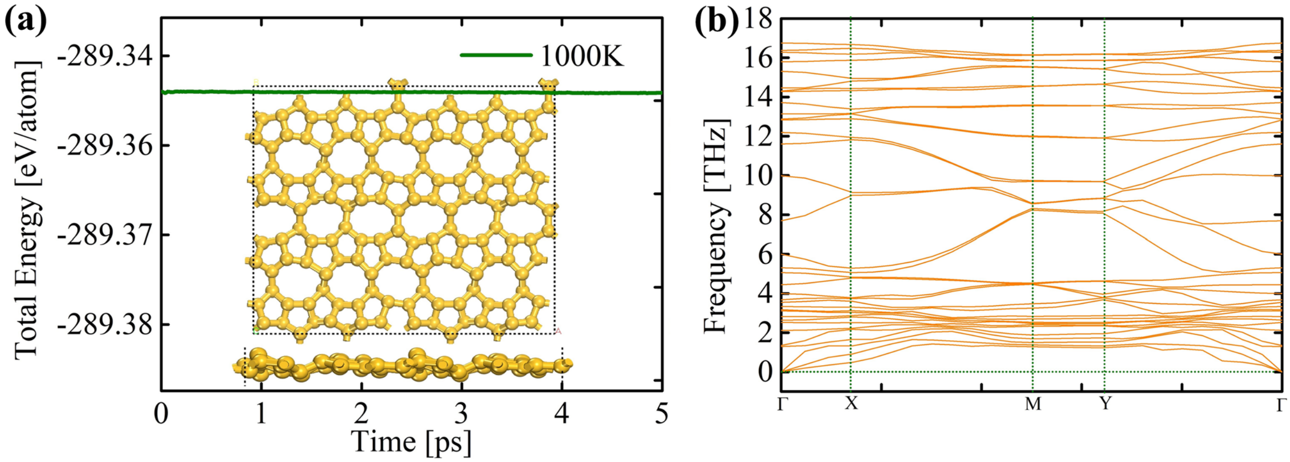

Figure 2. (**a**) Time evolution of the total energy per atom in the Pop-Si lattice at 1000K using the PBE approach. The insets show the top and side views of the final AIMD snapshot at 5 ps. (**b**) The phonon band structure of Pop-Si is calculated at the PBE level.

zone. This absence of imaginary frequencies confirms Pop-Si's dynamic stability, indicating that the structure is stable against small perturbations. The phonon dispersion curves also show no band gap between acoustic and optical modes, and the highest phonon frequency is approximately 16.86 THz. This value is close to the highest phonon frequency observed in silicene, about 17.98 THz[37], but significantly lower than the 48 THz found in Popgraphene[29]. Despite their distinct structural topologies, both Pop-Si and silicene exhibit comparable Si–Si bond energies, contributing to their similar vibrational properties. Additionally, the overlap between the acoustic and optical phonon bands in Pop-Si suggests strong inter-mode coupling, which is typical in silicon-based 2D materials[10,13,21,28]. This characteristic is advantageous for thermal conductivity applications, indicating efficient heat dissipation mechanisms.

The electronic properties of Pop-Si were thoroughly analyzed using the HSE06 method, providing deep insights into its conductive behavior, band structure, and electron localization characteristics. Figure 3 presents the electronic band structure (a), the partial density of states (PDOS) (b), and the electron localization function (ELF) (c) of Pop-Si. Figure 3a reveals no bandgap between the valence and conduction bands, indicating that Pop-Si is metallic, similar to Popgraphene[29]. This metallic behavior is evident along all the X-M path within the Brillouin zone. Pop-Si exhibits semiconducting behavior along other directions, highlighting the material's anisotropic electronic properties. This anisotropic conductance can be attributed to Pop-Si's unique structural features, particularly its buckled configuration and inherent ring topology. The distinct ring structures create preferential pathways for electron transport, contributing to the observed directional dependence of electrical conductivity.

The band structure also shows linear energy dispersions near the Fermi level near the X-M reciprocal points. This trend suggests that charge carriers in Pop-Si can propagate like massless Dirac fermions, a characteristic feature of materials with high electronic mobility and potential for high-speed electronic applications. The PDOS,

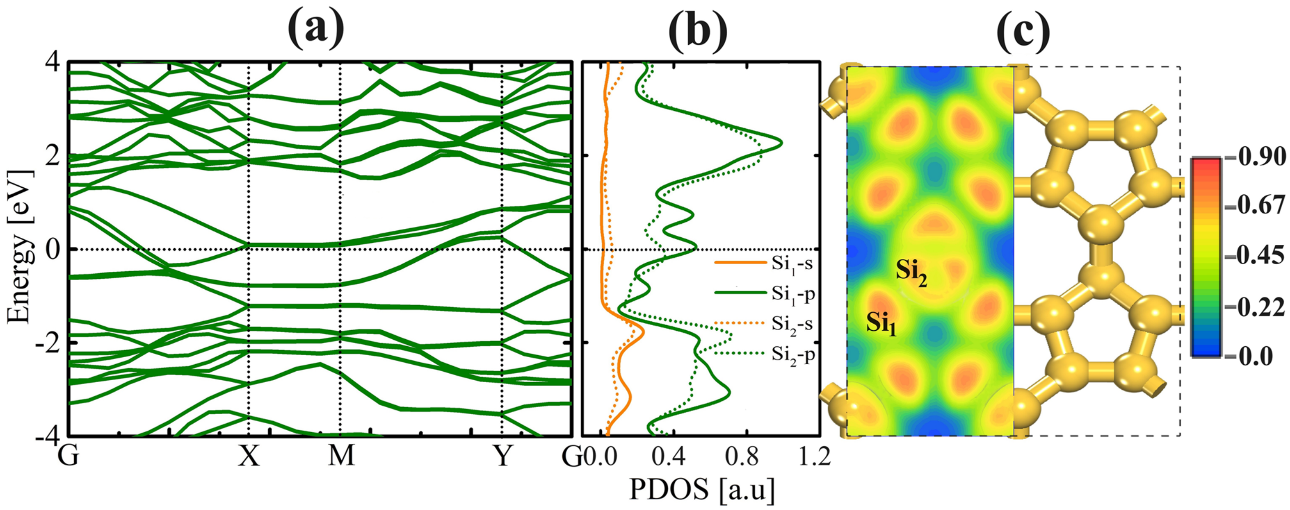

Figure 3. (**a**) Electronic band structure, (**b**) partial density of states (PDOS), and (**c**) electron localization function (ELF) for PH-Si. These properties were calculated using the HSE06 approach.

shown in Figure 3b, indicates that electronic states at the Fermi level are primarily derived from Si-p orbitals, with a smaller contribution from Si-s orbitals. This trend implies that p-orbitals drive electronic transitions and interactions in Pop-Si, reinforcing its metallic nature. When comparing Pop-Si with silicene and other 2D silicon allotropes, Pop-Si shows several similarities and notable differences. Silicene, for instance, also displays metallic behavior with a band structure dominated by Si-p orbitals at the Fermi level. However, the distinct anisotropic conductance observed in Pop-Si is less pronounced in silicene, which typically exhibits more isotropic electronic properties. The linear dispersion near the Fermi level in Pop-Si is similar to that observed in silicene, indicating the potential for high carrier mobility and applications in high-speed electronics.

Figure 3c provides a topological perspective on electron interactions (through the ELF), helping to understand the bonding characteristics within Pop-Si. ELF values range from 0 to 1, where values close to 1 indicate strong covalent interactions or lone pair electrons. In contrast, lower values around 0.5 suggest delocalization, ionic bonds, or weak van der Waals interactions. In Pop-Si, strong σ bonds are observed between Si atom pairs forming hexagons and pentagons, highlighted by intense orange regions with ELF values around 0.7. These strong covalent bonds contribute to localized electron interactions. In contrast, bonds between Si atoms forming the octagons are characterized by lighter-yellow areas with ELF values near 0.5, indicating a significant degree of electron delocalization. This coexistence of localized and delocalized electrons within the bond network of Pop-Si underpins its anisotropic conductance, as observed in the electronic band structure. Materials with delocalized valence electrons typically exhibit metallic-like conductivity. At the same time, those with strong covalent bonds tend to show semiconductor-like conductivity. The mixed bonding nature of Pop-Si results in its unique electronic properties, enabling both high electrical conductivity and anisotropic electronic behavior.

Now, we turn to the optical properties of Pop-Si, which reveal insights into its electronic structure and potential applications in optoelectronic devices. Figure 4 illustrates the optical characteristics of this material, considering different light polarizations and its inherent structural anisotropy. In this way, Fig. 4a shows that Pop-Si exhibits a high absorption coefficient of 10^4 cm^{-1}, primarily attributed to its metallic nature. The first absorption peaks for light polarized along the x (E//X) and y (E//Y) directions fall within the infrared spectrum, with the first peak occurring around 1.19 eV. This red-shift compared to silicene's absorption peak (around 2.9 eV)[21,45–47] suggests unique electronic transitions due to Pop-Si's structural and electronic differences. In the ultraviolet (UV) region, Pop-Si exhibits absorption peaks of approximately 4.4×10^4 cm^{-1} for E//X and 3.9×10^4 cm^{-1} for E//Y polarizations, at a photon energies of 4.7 eV and 4.9 eV, respectively. These values indicate Pop-Si's potential as a UV detector and absorber akin to silicene[47].

Figure 4b depicts Pop-Si's reflectivity across the infrared to UV regions. Pop-Si demonstrates relatively low reflectivity (below 0.2), with peaks around 0.09 and 0.06 for E//X and E//Y polarizations at photon energies (within the UV region) of 4.7 eV and 4.9 eV, respectively. This feature suggests efficient transmission of incident light in the UV-Vis range, with minimal reflection coefficients. The occurrence of reflection activity in the infrared region for in-plane polarization hints at Pop-Si's potential application as an infrared protector, similar to observations in silicene[45]. Moreover, Pop-Si exhibits anisotropic refractive indices along parallel and perpendicular polarizations to its basal plane, as illustrated in Fig.4c. This birefringent behavior indicates different velocities of light propagation in distinct polarization directions, a characteristic shared with silicene[48]. The refractive index data underscores Pop-Si's potential in optical polarization-sensitive devices.

Finally, we analyze the elastic properties of Pop-Si, focusing on the anisotropy in its mechanical behavior by determining Poisson's ratio ($\nu(\theta)$) and Young's modulus ($Y(\theta)$) under pressure within the xy plane. These properties are derived from established equations[49,50]:

$$Y(\theta) = \frac{C_{11}C_{22} - C_{12}^2}{C_{11}\alpha^4 + C_{22}\beta^4 + \left(\frac{C_{11}C_{22} - C_{12}^2}{C_{44}} - 2.0C_{12}\right)\alpha^2\beta^2} \tag{1}$$

and

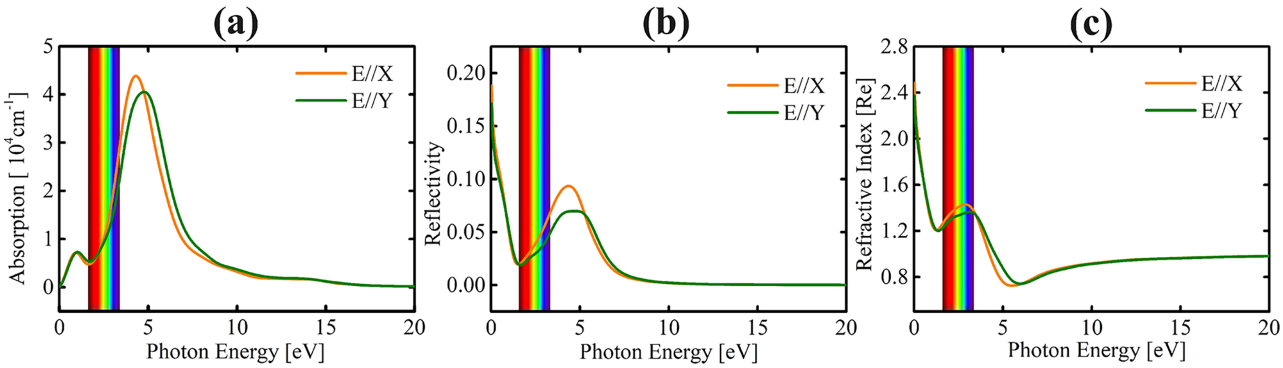

Figure 4. (**a**) optical absorption, (**b**) reflectivity, and (**c**) refractive index calculated at the HSE06 level for polarized light beams oriented along the x (E//X) and y (E//Y) directions relative to the surface of Pop-Si.

$$\nu(\theta)=\frac{(C_{11}+C_{22}-\frac{C_{11}C_{22}-C_{12}^2}{C_{44}})\alpha^2\beta^2-C_{12}(\alpha^4+\beta^4)}{C_{11}\alpha^4+C_{22}\beta^4+\left(\frac{C_{11}C_{22}-C_{12}^2}{C_{44}}-2.0C_{12}\right)\alpha^2\beta^2}. \tag{2}$$

where $\alpha=\cos(\theta)$ and $\beta=\sin(\theta)$. We have summarized the elastic constants and parameters in Table 1. Additionally, the distributions of Poisson's ratio (Fig. 5a) and Young's modulus (Fig. 5b) across its basal plane are visualized. These distributions indicate that the mechanical properties of Pop-Si are anisotropic. Importantly, the elastic constants agree with the Born-Huang criteria for orthorhombic crystals ($C_{11}C_{22}-C_{12}^2>0$ and $C_{44}>0$)[51,52], suggesting good mechanical stability.

For Young's modulus, we obtained a maximum value (Y_{MAX}) of 91.08 GPa, which is higher than the value reported for silicene (61.7 GPa)[22]. This discrepancy can be attributed to the inherent ring topology of Pop-Si, arising from the porosity imposed by the eight-atom rings and the rigidity of the bonds in fused pentagonal rings. These factors collectively contribute to the increased strain resilience of Pop-Si compared to its hexagonal counterpart, silicene. When subjected to compressive or tensile strain in one direction, materials typically exhibit expansion or contraction in the perpendicular direction, resulting in positive Poisson's ratios, which is the case for most ordinary materials. In Fig. 5, Pop-Si shows positive Poisson's ratios, with a maximum value (ν_{MAX}) of approximately 0.95. For this value, Young's modulus values remain below 20 GPa, indicating the incompressibility of Pop-Si under biaxial strains.

Common materials typically exhibit Poisson's ratios that fall within the range of 0.2 to 0.5[53]. A Poisson's ratio of 0.5 characterizes incompressible materials whose lateral dimensions do not change when subjected to axial strain. The minimal Poisson's ratios (ν_{MIN}) in Pop-Si under uniaxial strains along the x and y directions are 0.1 and 0.06, respectively. These values are notably lower than those observed in silicene, which is approximately 0.33 and 0.29[22]. Again, the reduced Poisson ratios in Pop-Si result from its lattice arrangement, which exhibits a higher degree of porosity than the honeycomb-based silicene lattice. This increased porosity allows Pop-Si to undergo more deformation under tension, resulting in lower Poisson ratios.

Discussion

In summary, we comprehensively investigated the properties of Pop-Si using first-principles calculations. Structurally, Pop-Si exhibits bond lengths and formation energy similar to other 2D silicon allotropes, suggesting experimental synthesizability. AIMD simulations at 1000K demonstrated that Pop-Si retains its structural integrity under high-temperature conditions, with no bond breakage observed, indicating robust thermal stability. The phonon dispersion curves show no imaginary frequencies, confirming Pop-Si's dynamical stability. The electronic band structure analysis revealed that Pop-Si is metallic, with no band gap between the valence and conduction bands. Anisotropic conductance was observed, attributed to the unique buckled structure and ring

Structure	C_{11}	C_{12}	C_{22}	C_{44}	Y_{MAX}	ν_{MAX}	ν_{MIN}
POP-Si	6.25	−0.55	91.80	20.93	91.8	0.95	0.006

Table 1. Elastic constants C_{ij} (GPa) and maximum values for Young's modulus (GPa) (Y_{MAX}) and maximum (ν_{MAX}) and (ν_{MIN}) Poisson's ratios.

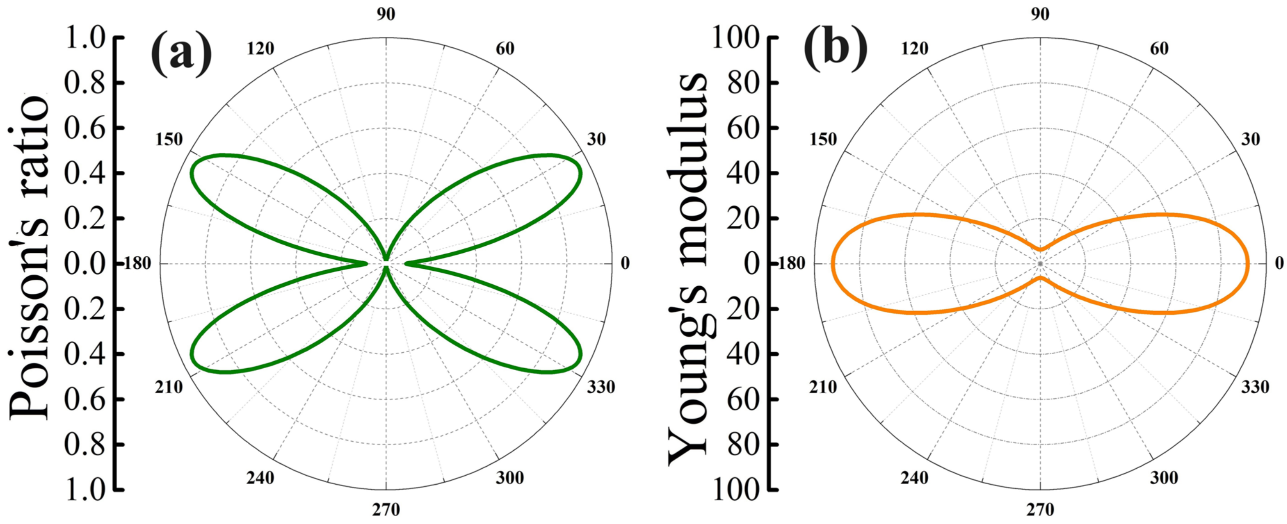

Figure 5. Schematic representation of (**a**) Poisson's ratio and (**b**) Young's modulus in the basal plane for Pop-Si.

topology. Linear energy dispersions near the Fermi level suggest that charge carriers in Pop-Si can propagate like massless Dirac fermions.

Pop-Si displays a high absorption coefficient in the visible to ultraviolet range, with significant peaks indicating potential applications as Vis-UV detectors and absorbers. The material also exhibits low to moderate reflectivity across the Vis-UV regions. It shows birefringence due to the anisotropic refractive index. The intrinsic electronic anisotropy and structural buckling of Pop-Si influence these optical properties. The analysis of elastic properties revealed anisotropy in Young's modulus and Poisson's ratio across the basal plane. Pop-Si showed a maximum Young's modulus of 91.80 GPa, higher than silicene due to its inherent porosity imposed by the octagonal rings and bond rigidity between silicon atoms forming the pentagonal rings. The material also exhibited positive Poisson's ratios, with values indicating incompressibility under biaxial strains. The reduced Poisson ratios compared to silicene are attributed to the higher degree of porosity in Pop-Si, allowing for more deformation under tension.

Methods

We conducted systematic DFT-based investigations into the mechanical, electronic, and optical properties of Pop-Si. The lattice structure is depicted in Fig. 1. All simulations were performed using the CASTEP code with norm-conserving pseudopotential for silicon[54]. We employed the Generalized Gradient Approximation (GGA) with the Perdew-Burke-Ernzerhof (PBE) functional[55], along with the Heyd-Scuseria-Ernzerhof (HSE06) hybrid functional[56] for enhanced accuracy. Electronic self-consistency was achieved using the Broyden-Fletcher-Goldfarb-Shannon (BFGS) algorithm[57,58]. A plane-wave basis set with an energy cutoff of 600 eV and a convergence criterion of 1.0×10^{-5} eV were used. Periodic boundary conditions ensured full lattice relaxation, with residual forces below 1.0×10^{-3} eV/Å and pressure under 1.0×10^{-2} GPa.

Lattice optimization was performed with a k-grid of $10 \times 10 \times 1$. For electronic and optical computations, k-grids of $15 \times 15 \times 1$ and $5 \times 5 \times 1$ were used for PBE and HSE06 methods, respectively. The phonon calculations considered a k-grid of $8 \times 8 \times 1$ for the PBE approach. The optical properties were determined using the approach presented in reference[59]. Partial Density of States (PDOS) calculations at the HSE06 level utilized a k-grid of 20 × 20 × 1. A vacuum region of 20 rA was implemented to avoid spurious interactions between periodic images. Phonon calculations were conducted using the linear response method with a grid spacing of 0.05 $Å^{-1}$, a convergence tolerance of 1.0×10^{-5} eV/$Å^2$, and a k-grid of $6 \times 6 \times 1$. Mechanical properties were evaluated using the stress-strain method based on the Voigt-Reuss-Hill approximation[60,61].

Data availability

Data supporting this study's findings are available upon reasonable request from the last author L.A.R.J.

Received: 14 June 2024; Accepted: 8 August 2024

References

1. Ieong, M., Doris, B., Kedzierski, J., Rim, K. & Yang, M. Silicon device scaling to the sub-10-nm regime. *Science* **306**, 2057–2060 (2004).
2. Srour, J., Marshall, C. J. & Marshall, P. W. Review of displacement damage effects in silicon devices. *IEEE Trans. Nucl. Sci.* **50**, 653–670 (2003).
3. Sun, C. *et al.* Single-chip microprocessor that communicates directly using light. *Nature* **528**, 534–538 (2015).
4. Flynn, M. J. & Hung, P. Microprocessor design issues: Thoughts on the road ahead. *IEEE Micro.* **25**, 16–31 (2005).
5. Andreani, L. C., Bozzola, A., Kowalczewski, P., Liscidini, M. & Redorici, L. Silicon solar cells: Toward the efficiency limits. *Adv. Phys.: X* **4**, 1548305 (2019).
6. Blakers, A., Zin, N., McIntosh, K. R. & Fong, K. High efficiency silicon solar cells. *Energy Procedia* **33**, 1–10 (2013).
7. Xu, M., Liang, T., Shi, M. & Chen, H. Graphene-like two-dimensional materials. *Chem. Rev.* **113**, 3766–3798 (2013).
8. Khan, K. *et al.* Recent developments in emerging two-dimensional materials and their applications. *J. Mater. Chem. C* **8**, 387–440 (2020).
9. Balendhran, S., Walia, S., Nili, H., Sriram, S. & Bhaskaran, M. Elemental analogues of graphene: Silicene, germanene, stanene, and phosphorene. *Small* **11**, 640–652 (2015).
10. Kara, A. *et al.* A review on silicene-new candidate for electronics. *Surf. Sci. Rep.* **67**, 1–18 (2012).
11. Houssa, M., Dimoulas, A. & Molle, A. Silicene: A review of recent experimental and theoretical investigations. *J. Phys.: Condens. Matter* **27**, 253002 (2015).
12. Geim, A. K. Graphene: Status and prospects. *Science* **324**, 1530–1534 (2009).
13. Zhao, J. *et al.* Rise of silicene: A competitive 2d material. *Prog. Mater Sci.* **83**, 24–151 (2016).
14. Oughaddou, H. *et al.* Silicene, a promising new 2d material. *Prog. Surf. Sci.* **90**, 46–83 (2015).
15. Kharadi, M. A. *et al.* Silicene: From material to device applications. *ECS J. Solid State Sci. Technol.* **9**, 115031 (2020).
16. Molle, A. *et al.* Silicene, silicene derivatives, and their device applications. *Chem. Soc. Rev.* **47**, 6370–6387 (2018).
17. Venkateshalu, S. *et al.* Phosphorene, antimonene, silicene and siloxene based novel 2d electrode materials for supercapacitors-a brief review. *J. Energy Storage* **48**, 104027 (2022).
18. Grazianetti, C., Cinquanta, E. & Molle, A. Two-dimensional silicon: The advent of silicene. *2D Mater.* **3**, 012001 (2016).
19. An, Y. *et al.* Recent advances and perspectives of 2d silicon: Synthesis and application for energy storage and conversion. *Energy Storage Mater.* **32**, 115–150 (2020).
20. You, Y., Yang, C., Zhang, X., Lin, H. & Shi, J. Emerging two-dimensional silicene nanosheets for biomedical applications. *Mater. Today Nano* **16**, 100132 (2021).
21. Chowdhury, S. & Jana, D. A theoretical review on electronic, magnetic and optical properties of silicene. *Rep. Prog. Phys.* **79**, 126501 (2016).
22. Mortazavi, B. *et al.* First-principles investigation of mechanical properties of silicene, germanene and stanene. *Physica E* **87**, 228–232 (2017).
23. Lima, K. & Junior, L. A. R. Unveiling a novel silicene-like material: A DFT study on pentahexoctite-silicon and its optoelectronic characteristics. *Comput. Condens. Matter* **39**, e00897 (2024).

24. Gorkan, T., Callioglu, S., Demirci, S., Akturk, E. & Ciraci, S. Functional carbon and silicon monolayers in biphenylene network. *ACS Appl. Electron. Mater.* **4**, 3056–3070 (2022).
25. Bafekry, A. *et al.* Two-dimensional silicon bismotide (sibi) monolayer with a honeycomb-like lattice: First-principles study of tuning the electronic propertiesF. *RSC Adv.* **10**, 31894–31900 (2020).
26. Fabris, G., Marana, N., Longo, E. & Sambrano, J. Porous silicene and silicon graphenylene-like surfaces: A dft study. *Theoret. Chem. Acc.* **137**, 1–9 (2018).
27. Chandiramouli, R., Srivastava, A. & Nagarajan, V. No adsorption studies on silicene nanosheet: Dft investigation. *Appl. Surf. Sci.* **351**, 662–672 (2015).
28. Aghdasi, P., Yousefi, S., Ansari, R. & Bagheri Tagani, M. A dft investigation on the mechanical and structural properties of silicene nanosheets under doping of transition metals. *Appl. Phys. A* **128**, 716 (2022).
29. Wang, S., Yang, B., Chen, H. & Ruckenstein, E. Popgraphene: A new 2d planar carbon allotrope composed of 5-8-5 carbon rings for high-performance lithium-ion battery anodes from bottom-up programming. *J. Mater. Chem. A* **6**, 6815–6821 (2018).
30. Álvarez-Zapatero, P., Herrero, A., Lebon, A., Gallego, L. & Vega, A. Ab initio study of lithium decoration of popgraphene and hydrogen storage capacity of the hybrid nanostructure. *Int. J. Hydrogen Energy* **46**, 15724–15737 (2021).
31. Thomas, S., Lee, C. H., Jana, S., Jun, B. & Lee, S. U. Phographene as a high-performance anode material with high specific capacity and fast li diffusion: From structural, electronic, and mechanical properties to lib applications. *J. Phys. Chem. C* **123**, 21345–21352 (2019).
32. Jiang, T. *et al.* Thermal conductivity of the popgraphene monolayer tailored by strain and defect: A molecular dynamics study. *Diam. Relat. Mater.* **130**, 109409 (2022).
33. Meng, F., Ni, M., Chen, F., Song, J. & Wei, D. Nanoscale fracture of defective popgraphene monolayers. *Phys. Chem. Chem. Phys.* **21**, 1242–1253 (2019).
34. Brandão, W., Aguiar, A., Ribeiro, L., Galvão, D. & De Sousa, J. On the mechanical properties of popgraphene-based nanotubes: A reactive molecular dynamics study. *ChemPhysChem* **22**, 701–707 (2021).
35. Mota, E. A. V., Moura-Moreira, M., Siqueira, M. R. S., da Silva, C. A. B. & Del Nero, J. Stability, edge passivation effect, electronic and transport properties of popgraphene nanoribbons. *Phys. Chem. Chem. Phys.* **23**, 2483–2490 (2021).
36. Pereira Junior, M. L. *et al.* Temperature effects on the fracture dynamics and elastic properties of popgraphene membranes. *ChemPhysChem* **21**, 1918–1924 (2020).
37. Cahangirov, S., Topsakal, M., Aktürk, E., Şahin, H. & Ciraci, S. Two- and one-dimensional honeycomb structures of silicon and germanium. *Phys. Rev. Lett.* **102**, 236804 (2009).
38. Wu, H. *et al.* Prediction of another semimetallic silicene allotrope with dirac fermions. *Phys. Lett. A* **381**, 3754–3759 (2017).
39. Aierken, Y., Leenaerts, O. & Peeters, F. M. A first-principles study of stable few-layer penta-silicene. *Phys. Chem. Chem. Phys.* **18**, 18486–18492 (2016).
40. Sheng, S. *et al.* The pentagonal nature of self-assembled silicon chains and magic clusters on ag (110). *Nano Lett.* **18**, 2937–2942 (2018).
41. Jung, J. H., Park, C.-H. & Ihm, J. A rigorous method of calculating exfoliation energies from first principles. *Nano Lett.* **18**, 2759–2765 (2018).
42. Kistanov, A. A. *et al.* Prediction of zn2 (v, nb, ta) n3 monolayers for optoelectronic applications. *J. Phys. Chem. Lett.* **14**, 11134–11141 (2023).
43. Martyna, G. J., Klein, M. L. & Tuckerman, M. Nosé-hoover chains: The canonical ensemble via continuous dynamics. *J. Chem. Phys.* **97**, 2635–2643 (1992).
44. Pun, G. P. & Mishin, Y. Optimized interatomic potential for silicon and its application to thermal stability of silicene. *Phys. Rev. B* **95**, 224103 (2017).
45. Bao, A., Li, X., Guo, X., Yao, H. & Chen, M. Tuning the structural, electronic, mechanical and optical properties of silicene monolayer by chemical functionalization: A first-principles study. *Vacuum* **203**, 111226 (2022).
46. Matthes, L., Pulci, O. & Bechstedt, F. Optical properties of two-dimensional honeycomb crystals graphene, silicene, germanene, and tinene from first principles. *New J. Phys.* **16**, 105007 (2014).
47. Das, R., Chowdhury, S., Majumdar, A. & Jana, D. Optical properties of p and al doped silicene: A first principles study. *RSC Adv.* **5**, 41–50 (2015).
48. John, R. & Merlin, B. Optical properties of graphene, silicene, germanene, and stanene from IR to far UV-a first principles study. *J. Phys. Chem. Solids* **110**, 307–315 (2017).
49. Wang, B., Wu, Q., Zhang, Y., Ma, L. & Wang, J. Auxetic b4n monolayer: A promising 2d material with in-plane negative Poisson's ratio and large anisotropic mechanics. *ACS Appl. Mater. Interfaces* **11**, 33231–33237 (2019).
50. Zhao, Y., Li, X., Liu, J., Zhang, C. & Wang, Q. A new anisotropic Dirac cone material: A b2s honeycomb monolayer. *J. Phys. Chem. Lett.* **9**, 1815–1820 (2018).
51. Mouhat, F. & Coudert, F. X. Necessary and sufficient elastic stability conditions in various crystal systems. *Phys. Rev. B* **90**, 224104. https://doi.org/10.1103/PhysRevB.90.224104 (2014).
52. Ying, Y., Fan, K., Zhu, S., Luo, X. & Huang, H. Theoretical investigation of monolayer RHTECL semiconductors as photocatalysts for water splitting. *J. Phys. Chem. C* **124**, 639–646. https://doi.org/10.1021/acs.jpcc.9b09593 (2020).
53. Greaves, G. N., Greer, A. L., Lakes, R. S. & Rouxel, T. Poisson's ratio and modern materials. *Nat. Mater.* **10**, 823–837 (2011).
54. First principles methods using castep. *Zeitschrift für kristallographie-crystalline materials* **220**, 567–570 (2005).
55. Perdew, J. P., Burke, K. & Ernzerhof, M. Generalized gradient approximation made simple. *Phys. Rev. Lett.* **77**, 3865 (1996).
56. Heyd, J., Scuseria, G. E. & Ernzerhof, M. Hybrid functionals based on a screened coulomb potential. *J. Chem. Phys.* **118**, 8207–8215 (2003).
57. Head, J. D. & Zerner, M. C. A broyden-fletcher-goldfarb-shanno optimization procedure for molecular geometries. *Chem. Phys. Lett.* **122**, 264–270 (1985).
58. Pfrommer, B. G., Côté, M., Louie, S. G. & Cohen, M. L. Relaxation of crystals with the quasi-newton method. *J. Comput. Phys.* **131**, 233–240 (1997).
59. Lima, K. L. & Junior, L. R. A DFT study on the mechanical, electronic, thermodynamic, and optical properties of GAN and ALN counterparts of biphenylene network. *Mater. Today Commun.* **37**, 107183 (2023).
60. Zuo, L., Humbert, M. & Esling, C. Elastic properties of polycrystals in the Voigt-Reuss-Hill approximation. *J. Appl. Crystallogr.* **25**, 751–755 (1992).
61. Chung, D. H. & Buessem, W. R. The Voigt-Reuss-hill approximation and elastic moduli of polycrystalline MgO, CaF2, β-ZnS, ZnSe, and CdTe. *J. Appl. Phys.* **38**, 2535–2540 (2004).

Acknowledgements

This work was financed by the Coordenação de Aperfeiçoamento de Pessoal de Nível Superior (CAPES), Conselho Nacional de Desenvolvimento Cientifico e Tecnológico (CNPq), and Fundação de Apoio à Pesquisa do Distrito Federal (FAP-DF). L.A.R.J. acknowledges the financial support from FAP-DF grant 00193 − 00001857/2023 − 95 and FAPDF-PRONEM grant 00193.00001247/2021 − 20, and CNPq grant

350176/2022 — 1. L.A.R.J. acknowledges Núcleo de Computação de Alto Desempenho (N.A.C.A.D.) and for providing the computational facilities. This work used Centro Nacional de Processamento de Alto Desempenho em São Paulo (CENAPAD-SP) resources. L.A.R.J. and K.A.L.L. also acknowledge CAPES for partially financing this study - Finance Code 88887.691997/2022-00. F.L.L.M. and D.A.S. acknowledge General Attorney of the Union - AGU grant 697.935/2019.

Author contributions

K.A.L.L, D.A.S., and F.L.L.M.: Data curation, Formal analysis, Methodology, Prepared Figures, and Writing - Original draft preparation. F.L.L.M., R.G., and L.A.R.J.: Conceptualization, Funding acquisition, and Writing - Reviewing and Editing. All authors reviewed the manuscript.

Conflict of interest

The authors declare no conflict of interests.

Additional information

Supplementary information is available for this paper at https://doi.org/10.1038/s41598-024-69788-4.

Correspondence and requests for materials should be addressed to L.A.R.J.

Reprints and permissions information is available at www.nature.com/reprints.